Science Press

ARTICLE

Effect of Mn Addition on Microstructure and Corrosion Behavior of Extruded Mg-Zn-Y-Nd Alloy

Liu Baosheng[1],   Wang Yaning[1],   Zhang Yuezhong[1],   Hou Lifeng[2],   Wei Yinghui[1, 2]

[1] Taiyuan University of Science and Technology, Taiyuan 030024, China; [2] Taiyuan University of Technology, Taiyuan 030024, China

Abstract: Effect of Mn addition on the microstructure and corrosion behavior of extruded Mg-Zn-Y-Nd alloy immersed in 3.5 wt% NaCl solution was studied by optical microscope, scanning electron microscope equipped with energy dispersive spectroscope, X-ray diffraction, immersion, and electrochemical measurements. Results suggest that the Mn addition in the studied Mg-Zn-Y-Nd alloy can induce $Mg_3Y_2Zn_3$ (*I*-phase) precipitation which may inhibit dynamic recrystallizaiton (DRX) grain coarsening during hot extrusion. Meanwhile, its corrosion resistance is improved by the addition of Mn. The corrosion rates of free and 1.0 wt% Mn containing Mg-5.6Zn-1Y-0.4Nd alloys are 18.78 and 9.89 $mm·a^{-1}$, respectively. The improvement of corrosion resistance is mainly due to an enhanced protectiveness of the corrosion product layer.

Key words: Mg-Zn-Y-Nd alloy; Mn addition; microstructure; dynamic recrystallizaiton (DRX); corrosion resistance

Magnesium (Mg) alloy is a candidate metal for structural materials, because of its merits of light weight, high specific strength, excellent creep resistance, excellent casting performance and considerable age hardening response[1,2]. However, its low strength, limited ductility and poor corrosion resistance put a constraint on their widespread applications[3].

Mg-Zn-Y series alloy is one of the most desirable magnesium alloys for industrial applications because of the strengthened LPSO phases such as *X*-phase, *W*-phase and *I*-phase[4-6]. Recently, neodymium (Nd) acts as an important alloying element in magnesium alloys and the effect of Nd addition on the structure and properties of Mg-Zn-Y alloys have been investigated[7,8]. Wu et al.[9] and Zhou et al.[10] reported that the strengthening mechanism of the mixed Nd and Y addition is significantly better than that of the single Nd at various temperatures. Thus, Mg-Zn-Y-Nd alloy has attracted extensive attention. However, poor corrosion resistance of Mg-Zn-Y-Nd alloy inevitably hinders their widespread applications, and the researchers have endeavored to find a solution to overcome this issue.

Mn addition has also demonstrated to be effective in enhancing corrosion resistance of Mg-Al, Mg-Zn, Mg-Ca and Mg-Sn alloys[11-16]. As well known, a small amount of manganese can improve the properties of the alloys because the formation of Al-Mn-Fe intermetallic phase can reduce harmful impurities (Fe)[17,18]. However, the effect of Mn addition on corrosion resistance of Mg-Zn-Y-Nd alloy is rarely investigated[19].

The main objective of this work is to study the effect of Mn addition on the microstructure of Mg-5.6Zn-1Y-0.4Nd alloy during the extrusion. Further, the corrosion behavior and mechanism of the Mg-5.6Zn-1Y-0.4Nd (wt%) alloys with and without 1.0 wt% Mn were investigated in 3.5 wt% NaCl solution. This will help the development of lightweight magnesium material for automobile and electronic industries.

1   Experiment

1.1 Material preparation

Alloys with nominal compositions (wt%) of the Mg-5.6Zn-1Y-0.4Nd (ZYN) alloy and the Mg-5.6Zn-1Y-0.4Nd-1Mn (ZYNM) alloy were prepared by dissolving high-pure magnesium, pure Zn, Mg-30%Y, Mg-30%Nd and Mg-4.1%Mn master alloys. The raw materials were melted with a mild steel crucible in an electric resistance furnace. Melt course was protected by the RJ-2 flux and subsequent pouring into a steel mould by pre-heating to 473 K. The alloy composition analyzed is listed in Table 1. Cast ingots with 90 mm-diameter and 200 mm-length were homogenized at 673 K for 24 h. The rectangular solid materials with 12 mm in width and 6 mm in thickness were machined by indirect extrusion at the initial temperature of 573 K, an average extrusion velocity as 1 m/min, and an extrusion ratio as 30:1.

1.2 Microstructure characterization

The specimens for microstructure characterization were etched with a solution of 5 mL acetic acid, 5.5 g picric acid, 10 mL distilled water, and 90 mL ethanol. The microstructure of the alloys and corroded surface morphology were characterized by scanning electron microscopy (SEM, Hitachi S-4800) equipped with energy dispersive X-ray spectroscopy (EDS). The phase compositions were investigated using X-ray diffraction (XRD, Rigaku D/MAX-2500PC).

1.3 Immersion and electrochemical measurements

Corrosion behaviour of the alloys was tested using immersion (hydrogen evolution), weight loss, and electrochemical measurement technology in 3.5 wt% NaCl solution at 298 K. After the immersion test, the sample surfaces were washed with a solution of 200 g/L CrO₃ and then the weight loss of the sample was measured. The H_2 volume measurements were tested according to the method proposed by Song and Atrens[20]. The consequence of the H_2 volume and weight loss after immersion test 72 h were taken from the average of three replicates of each alloy. Electrochemical tests were performed using a universal three-electrode cell with working electrode (sample), a platinum counter electrode and an Ag/AgCl reference electrode. Open circuit potential (OCP) measurement were conducted in 3.5 wt% NaCl solution for 1200 s before the polarization measurements. The polarization measurements were conducted with 0.5 mV/s. Electrochemical impedance spectroscopy (EIS) measurements were conducted in the frequency range from 10^5 to 10^{-2} Hz with a sinusoidal signal perturbation.

2 Results and Discussion

2.1 Microstructure

Fig.1 is the microstructures of the ZYN and ZYNM alloys. In addition to large amounts of undissolved second phase particles, it has been found that the microstructures are mainly composed of α-Mg grains, which may originate from dynamic recrystallization (DRX) during extrusion. Meanwhile, the average size of the α-Mg grains in ZYNM (~7.8 μm) is smaller than that in ZYN (~11.6 μm). This suggests that the Mn element plays an important role in grain refinement in Mg-Zn-Y-Nd alloy during process of dynamic recrystallization, which corresponds well with previous reports[10]. This is mainly because Mn can induce $Mg_3Y_2Zn_3$ (*I*-phase) precipitation, which is stable at high temperature[2]. The precipitation may inhibit grain growth during hot extrusion. Additionally, the migration of grain boundaries also can be effectively prevented by granular Mn. Therefore, it can be concluded that the addition of Mn can significantly refine the grain of as-extruded Mg-Zn-Y-Nd alloy.

The XRD analysis results of the as-extruded ZYN and ZYNM alloys are shown in Fig.2. Besides the strong diffraction peaks of α-Mg substrate, the featured diffraction peaks for *I*-(Mg_3Zn_6(Y, Nd)) phase are observed in the extruded alloys. In addition, addition of Mn to Mg-Zn-Y-Nd system did not contribute to new phase formation but refined grains, which is consistent with Mg-Mn, Mg-Zn-Mn and Mg-Y-Mn phase diagrams reports [21,22].

Fig.3a and 3b are the SEM morphologies of the ZYN and ZYNM alloys. The bright second phases particles are

Table 1   Chemical compositions of the extruded alloys (wt%)

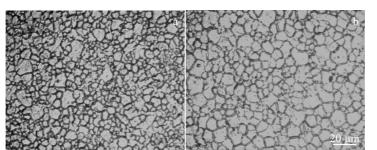| Alloy	Zn	Y	Nd	Mn	Fe	Si	Cu	Ni	Mg
ZYN	5.45	1.35	0.39	-	0.001	0.003	0.001	0.001	Bal.
ZYNM	5.48	1.42	0.38	0.95	0.001	0.004	0.001	0.001	Bal.

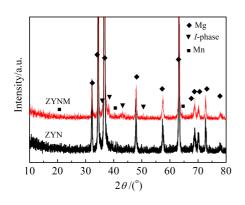Fig.1   Optical micrographs of ZYN (a) and ZYNM (b) alloys

Fig.2   XRD patterns of the extruded alloys

observed in the both ZYN and ZYNM alloys which are denser in the ZYNM alloy. Additionally, the size of second phase particles is more uniform, and the particles in Mg matrix are of uniform distribution in the ZYNM alloy. The chemical composition of these phases in both extruded alloys, as indicated in Fig.3c and 3d, includes Mg, Zn, Y and Nd. The second phase can be inferred as *I* phase because the Zn/RE atomic ratio is close to 6, which is in agreement with the XRD results. Thus, in this study, the formed phase in the extruded alloys is *I*-phase, which is similar to the previous reports[23]. What's more, Mn element is also observed in ZYNM alloy, which indicates the presence of Mn. These lead to grains refinement by inhibition of the migration of grain boundaries during hot extrusion.

2.2   Corrosion behavior

The corrosion behaviors of the extruded alloys were investigated by immersion and electrochemical tests. Weight loss and H_2 volume amounts of the extruded alloys in 3.5wt% NaCl solution at 298 K are shown in Fig.4, in which both the weight loss and the H_2 volume amounts of the ZYNM alloy are significantly smaller than those of the ZYN alloy, directly indicating that the latter is much less corrosive than the former in the current corrosive environment. For ZYN and ZYNM alloys, the weight loss were 15.67 and 5.85 mg·cm^{-2} while the quantities of the collected H_2 volume were 25.23 and 12.9 mL·cm^{-2}, respectively. The corresponding corrosion rates were 18.78 and 9.89 mm·a^{-1} for the ZYN and ZYNM alloys using the following conversions: corrosion rate (mm/a) =2.10 (weight loss rate (mg·cm^{-2}·d^{-1}))[24].

Fig.5 shows the corrosion evolution of the ZYN and ZYNM alloys, after the immersion test in 3.5% NaCl solution at 25 ºC. In general, both alloys underwent localized corrosion. After immersion for only 5 min, both alloys lost metallic luster due to the formation of corrosion product films. With the immersion time prolonging, the color of the alloy surface gradually deepened. Immersion time until 30 min, white corrosion pits were found to form first in the both alloys surface, and more corrosion pits were observed on ZYN alloy surface. After immersion for 1 h, the surfaces of both alloys were darker and some areas become brown. With the corrosion processing, the brown corrosion area expended and presented a different distribution until immersion for 3 h.
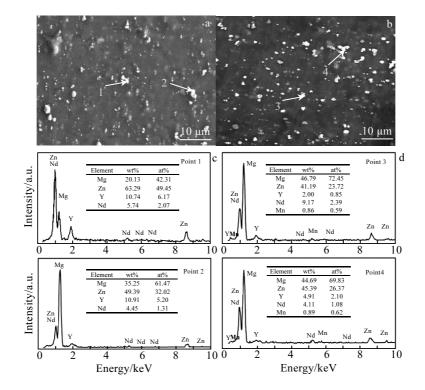

Fig.3   SEM micrographs of the ZYN (a) and ZYNM (b) alloys; EDS results of points marked in Fig.3a (c) and in Fig.3b (d)

Specifically, ZYN alloy shows dispersed corrosion area, presenting a striking contrast to the continuous corrosion area of ZYNM alloy.

In order to further explore the corrosion morphology of ZYN and ZYNM alloy after immersion for 3 h, the microscopic morphology of brown corroded area (Fig.5) was examined by SEM and the results are shown in Fig.6. As for ZYN alloy, a number of loose corrosion products and pores can be observed (Fig.6a). From the high-magnification SEM image (Fig.6b), loose and irregular particles have piled up on the surface. The surface of ZYNM alloy is different from the ZYN alloy surface obviously; uneven but relatively compact corrosion products are observed (Fig.6c). From the high-magnification SEM image (Fig.6d), irregular and compact protrusions accumulate on the surface, which indicates that the films can provide a good protection. Comparing the corrosion morphology of the two alloys, it can be deduced that the addition of Mn can significantly improve

the integrity and compactness of the corrosion product film, thereby affecting the corrosion process and improving the corrosion resistance of the alloy, which is sufficiently in accordance with the results obtained from the EIS tests.
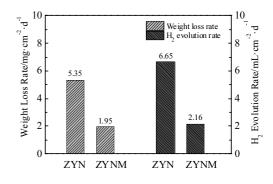

Fig.4   Weight loss and H_2 volume values of the ZYN and ZYNM alloys after immersion for 72 h in 3.5wt% NaCl solution
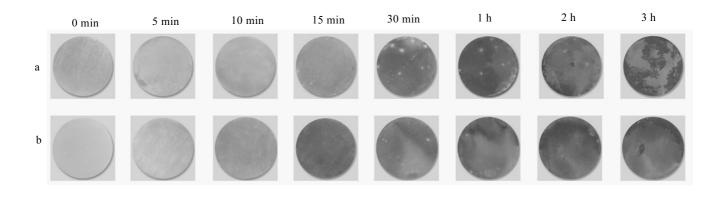

Fig.5   Optical micrographs of the extruded alloys after immersion for various time in 3.5wt% NaCl solution: (a) ZYN and (b) ZYNM
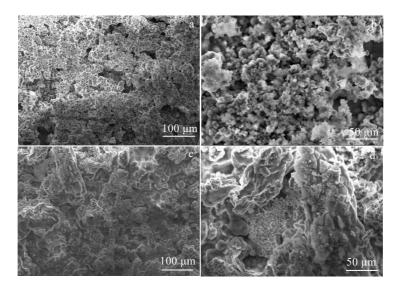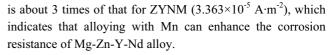

Fig.6   SEM morphologies of the corroded surface of ZYN alloy (a, b) and ZYNM alloy (c, d) in 3.5wt% NaCl solution after immersion at 25 ºC for 3 h
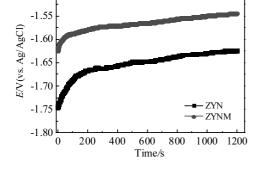
Fig.7 presents the OCP variations of extruded alloys upon immersion in 3.5 wt% NaCl solutions; these curves were measured for 1200 s before the start of the polarization test. In general, the value of OCP seems to increase in a parabolic shape. The OCPs are very negative at the immersion beginning, and shift towards the positive direction in about the first 130 s immersion. After the initial fast increase stage, the OCPs of ZYN and ZYNM alloys slowly increase constantly and reach stability eventually. The relatively stable OCP of ZYN is more negative than that of ZYNM. Generally, the OCP variations are assumed to correlate with the formation, dissolution and protection ability of the surface film of the alloys. The increased OCP in parabolic shape indicates the formation of the corrosion product film with immersion time[25,26]. No passivity breakdown was observed when the immersion time was less than 1200 s. The OCP variations of ZYNM alloys described above reflect that addition of Mn enhances the stability of the alloy surface film, which is expected to the improvement of the alloy in the corrosion resistance.

The electrochemical polarization curves of the extruded alloys in 3.5wt% NaCl solution at 25 ºC are shown in Fig.8. It shows that the cathodic polarization behavior of the alloys has little effect on the Mn alloying. On the other hand, the addition of Mn greatly affects the anodic polarization behavior of the alloy. The corrosion potential (E_{corr}), pitting potential (E_{pit}) and the corrosion current density (i_{corr}) are obtained from the polarization curves by Tafel fitting. The corresponding results are also presented in Fig.8. The E_{corr} of the ZYN alloys (-1.587 V) shifts slightly in the positive direction compared to that of the ZYNM (-1.532 V). Since the difference in cathode reaction rate of the alloy is small, it can be considered that the addition of Mn increases the stability of the passivation film and leads to an increase in the E_{corr} value. What's more, an obvious pitting phenomenon appears in its anodic polarization curve of the ZYN alloy (-1.476 V) and ZYNM alloy (-1.478 V), which indicate the both alloys suffer localized corrosion and which shows similar corrosion resistance to chloride pitting. Furthermore, the i_{corr} of the ZYN (9.954×10^{-5} A·cm^{-2})

is about 3 times of that for ZYNM (3.363×10^{-5} A·m^{-2}), which indicates that alloying with Mn can enhance the corrosion resistance of Mg-Zn-Y-Nd alloy.

To further investigate the corrosion resistance of extruded alloys in 3.5 wt% NaCl solution, EIS measurements were carried out, and Fig.9 shows the corresponding results. Nyquist plots exhibit a high frequency (HF) and a low frequency (LF) capacitive loops, which can be observed in the Nyquist plots (Fig.9a). Moreover, a small part of the deformed inductive loop appears at the much lower frequencies, which might be related with the existence of relaxation process of absorbed species, such as Mg(OH)$_{ads+}$ or Mg(OH)$_2$[27,28]. It is well known that HF capacitor loops are attributed to charge transfer reactions at the interface between the metal surface and the corrosive medium, which can be described by charge transfer resistance (R_t) and a constant phase element (CPE)[29,30]. CPE is always used to improve the fitting precision, which describes the non-ideal capacitive behavior of the electric double layer[30,31] caused by the interface microscopic roughness[32,33]. The LF capacitive loop is generally related to the mass transport in solid phase, i.e. to the diffusion of ions through the hydroxide or oxide film[34], or to the stable, allitic passivating film forming on I phase surface, which can be assigned with CPE$_f$ (a film capacity) and R_f (a film resistance)[35]. The presence of low frequency inductive loop is due to the initiation of localized corrosion[36]. The impedance and frequency Bode plots (Fig.9b) shows that the impedance values of ZYN rapidly increase with the Mn addition, which means that the corrosion resistance of the surface film is improved with the alloying of Mn. This is consistent with the dimension variations of the Nyquist plots. As for the Bode plot (Fig.9b), two wave crests and one trough are observed of ZYN and ZYNM alloys, implying the existence of three time constants (two capacitance loops and one inductance loop).

To further explore the corrosion mechanism of the alloys from EIS measurements, the EIS spectra of extruded alloys shown in Fig.9 can be characterized by the equivalent circuit shown in Fig.10. The corrosive medium resistance R_s is in series with the complex elements of R_t and CPE, and in series

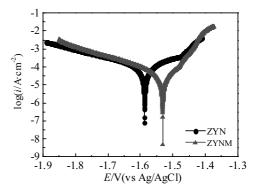Fig.7　OCP variations of extruded alloys upon immersion in 3.5 wt% NaCl solution

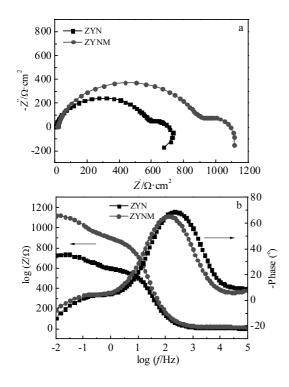Fig.8　Polarization curves of ZYN and ZYNM alloys in 3.5 wt% NaCl solution

Fig.9   Electrochemical impedance spectra of extruded alloys in 3.5 wt% NaCl solution: (a) Nyquist plots and (b) Bode plots

with the complex elements of CPE_f and R_f. R_t represents the charge transfer resistance, while CPE_{dl} represents the electric double layer capacity at the interface of Mg substrate and electrolyte solution, which is defined by Y_0 and n. CPE_f and R_f represent the capacity and resistance of the corrosion product film formed in NaCl solution, respectively. CPE_f is defined by Y_f and n_f. R_L and L represent the inductance resistance and inductance, respectively, which are used to describe the low-frequency inductance loop. The corrosion processes of

both alloys are similar owing to the similar spectra shape, while the alloys show different corrosion resistances. Table 2 shows EIS parameters of the extruded alloys in 3.5wt% NaCl at their respective open circuit potentials. Compared with ZYN alloy, the Mn-containing ZYNM alloys have larger R_t values, which indicates that Mn addition is helpful for improving the corrosion resistance. Additionally, the ZYNM has bigger R_f values, which suggests that addition of Mn impairs the stability of the film on ZYN alloy surface. From comprehensive evaluation of the R_t and R_f variations, the ZYNM alloy is expected to have high corrosion resistance and good anti-corrosive performance.

Based on the above results, the improved corrosion resistance of ZYNM alloy resulting from Mn addition can be ascribed to the following two aspects. Firstly, Mn alloying could enhance the protectiveness of the corrosion product layer, resulting in relatively larger resistance in corrosion process. Secondly, refined grain in the ZYNM alloy reduces corrosion rate. The smaller the grain size, the more the grain boundaries. The grain boundaries act as a physical corrosion barrier in corrosive medium to slow down the corrosion rate compared with coarse-grained ZYN alloy[37,38].
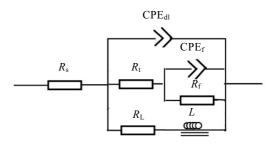

Fig.10   Equivalent circuit used in the analysis of EIS shown in Fig.9

Table 2   EIS parameters of the extruded alloys in 3.5wt% NaCl at their respective open circuit potentials

Alloy	$R_s/\Omega\cdot cm^2$	$Y_0/\Omega^{-1}\cdot cm^{-2}\cdot s^{-1}$	n	$R_t/\Omega\cdot cm^2$	$Y_f/\Omega^{-1}\cdot cm^{-2}\cdot s^{-1}$	n_f	$R_f/\Omega\cdot cm^2$	$L/H\cdot cm^{-2}$	$R_L/\Omega\cdot cm^2$
ZYN	7.582	1.79×10^{-5}	0.933	562.2	5.09×10^{-3}	0.754	163.1	37780	123.1
ZYNM	18.92	1.69×10^{-5}	0.914	861.4	5.13×10^{-3}	0.696	274.7	92520	276.1

3   Conclusions

1) Alloying with Mn can obviously refine the dynamic recrystallizaiton (DRX) grain size of the Mg-Zn-Y-Nd alloy.

2) The corrosion resistance of the Mg-Zn-Y-Nd alloy is found to be increased by alloying with Mn. The corrosion rates in 3.5 wt% NaCl solution at 298 K are 9.89 and 18.78 mm·a^{-1} for the ZYNM and ZYN alloys, respectively. The improved corrosion resistance with the addition of Mn is attributed to the enhanced protectiveness of the corrosion

products layer, as well as to physical corrosion barrier resulting from more grain boundaries due to grain refinement.

References

1 Peng Q M, Ge B C, Fu H *et al. Nanoscale*[J], 2018, 10: 18 028

2 Ślęzak M, Bobrowski P, Rogal Ł *et al. Journal of Materials Engineering and Performance*[J], 2018, 27: 4593

3 Liu B S, Kuang Y F, Fang D Q *et al. International Journal of Materials Research*[J], 2017, 108: 262

4 Kawamura Y, Hayashi K, Inoue A *et al. Materials Transactions*[J], 2001, 42: 1172

5 Guo Y P, Wang Y N, Zhang M G *et al. International Journal of Materials Research*[J], 2018, 109: 944

6 Tahreen N, Zhang D F, Panb F S *et al. Journal of Materials Science & Technology*[J], 2018, 34: 1110

7 Lan A, Huo L. *Material Science and Engineering A*[J], 2016, 651: 646

8 Li Q, Wang Q D, Wang Y X *et al. Journal of Alloys and Compounds*[J], 2007, 427: 115

9 Wu A R, Xia C Q. *Materials Design*[J], 2007, 28: 1963

10 Zhou H T, Zhang Z D, Liu C M *et al. Materials Science and Engineering A*[J], 2007, 445: 1

11 Zhang Y Z, Wang X Y, Liu B S *et al. International Journal of Materials Research*[J], 2018, 109: 1

12 Mingo B, Arrabal R, Mohedano M *et al. Material & Design*[J], 2017, 130: 48

13 Nam N D, Mathesh M, Forsyth M *et al. Journal of Alloys and Compounds*[J], 2012, 542: 199

14 Bakhsheshi-Rad H R, Idris M H, Abdul-Kadir M R *et al. Material & Design*[J], 2014, 53: 283

15 Cho D H, Lee B W, Park J Y *et al. Joural of Alloys and Compounds*[J], 2017, 695: 1166

16 Ha H Y, Kim H J, Baek S M *et al. Scripta Materialial*[J], 2015, 109: 38

17 Gandel D, Easton M, Gibson M *et al. Corrosion Science*[J], 2012, 69: 666

18 Wang J, Huang S, Li Y *et al. Materials Science and Engineering: C*[J], 2013, 33: 3832

19 Zhou Y L, Li Y, Luo D M *et al. Materials Science and Engineering: C*[J], 2015, 49: 93

20 Zhao M C, Liu M, Song G *et al. Advanced Engineering Materials*[J], 2008, 10: 93

21 Massalski T, Okamoto H. *Binary Alloy Phase Diagrams*[M]. USA: ASM International, 1990

22 Effenberg G, Aldinger F, Rokhlin L. *Ternary Alloys*[M]. Stuttgart: MSI, 1999

23 Uhlig H H, Revie R W. *Corrosion and Corrosion Control, Third Ed* [M]. New York: John Wiley, 1985

24 Zhang L, Zhou W, Hu P H *et al. Journal of Alloys and Compounds*[J], 2016, 688: 868

25 Ha H Y, Kang J Y, Yang J *et al. Corrosion Science*[J], 2013, 75: 426

26 Ha H Y, Kang J Y, Kim S G *et al. Corrosion Science*[J], 2014, 82: 369

27 Wu G S, Zhao Y, Zhang X M *et al. Corrosion Science*[J], 2013, 68: 279

28 He M F, Liu L, Wu Y T *et al. Corrosion Science*[J], 2008, 50: 3267

29 Liu N, Wang J L, Wang L D *et al. Corrosion Science*[J], 2009, 51: 1328

30 Feliu S, Maffiotte C, Samaniego A *et al. Electrochimica Acta*[J], 2011, 56: 4554

31 Brett C M A, Dias L, Trindade B *et al. Electrochimica Acta*[J], 2006, 51: 1752

32 Guo X W, Chang J W, He S M *et al. Electrochimica Acta*[J], 2007, 52: 2570

33 Song Y W, Han E H, Dong K H *et al. Corrosion Science*[J], 2014, 88: 215

34 Hagihara K, Okubo M, Yamasaki M *et al. Corrosion Science*[J], 2016, 109: 68

35 Song Y W, Shan D Y. *Corrosion Science*[J], 2009, 51: 1087

36 Wang S D, Xu D K. *Corrosion Science*[J], 2015, 92: 228

37 Aung NaingNaing, Zhou Wei.*Corrosion Science*[J], 2010, 52: 589

38 Argade G R, Panigrahi S K, Mishra R S. *Corrosion Science*[J], 2012, 58: 145

Mn 添加对挤压态 Mg-Zn-Y-Nd 合金微观组织和腐蚀行为的影响

刘宝胜[1]，王亚宁[1]，张跃忠[1]，候利锋[2]，卫英慧[1, 2]
(1. 太原科技大学 材料科学与工程学院，山西 太原 030024)
(2. 太原理工大学 材料科学与工程学院，山西 太原 030024)

摘　要：通过光学显微镜，配备能量色散谱仪的扫描电子显微镜，X射线衍射仪，浸泡法和电化学测试的方法研究了Mn的添加对挤压Mg-Zn-Y-Nd合金在3.5%（质量分数）NaCl溶液中的微观组织和腐蚀行为的影响。结果表明，在研究的Mg-Zn-Y-Nd合金中添加Mn可以诱导$Mg_3Y_2Zn_3$（I相）沉淀，可以抑制热挤压过程中动态再结晶（DRX）晶粒的粗化。同时，添加了Mn也可以提高合金的耐腐蚀性。不含Mn的Mg-5.6Zn-1Y-0.4Nd合金与含锰1.0%的Mg-5.6Zn-1Y-0.4Nd合金腐蚀速率分别为18.78和9.89 mm·a^{-1}。而耐腐蚀性的提高主要归因于腐蚀产物层保护性的增强。
关键词：Mg-Zn-Y-Nd合金；Mn含量；微观组织；动态再结晶；耐腐蚀性

作者简介：刘宝胜，男，1979 年生，博士，副教授，太原科技大学材料科学与工程学院，山西 太原 030024，电话：0086-351-6998256，E-mail: liubaosheng@tyust.edu.cn; 13903410545@163.com